Journal of Alloys and Compounds 514 (2012) 76–80

Contents lists available at SciVerse ScienceDirect

Journal of Alloys and Compounds

journal homepage: www.elsevier.com/locate/jallcom

A magnetite nanocrystal/graphene composite as high performance anode for lithium-ion batteries

Xiaodan Huang[a,b], Xufeng Zhou[c], Kun Qian[b], Dongyuan Zhao[a], Zhaoping Liu[c,*], Chengzhong Yu[a,b,**]

[a] Department of Chemistry, Fudan University, Shanghai 200433, PR China
[b] ARC Centre of Excellence for Functional Nanomaterials and Australian Institute for Bioengineering and Nanotechnology, The University of Queensland, Brisbane, QLD 4072, Australia
[c] Ningbo Institute of Material Technology and Engineering, Chinese Academy of Sciences, Ningbo 315201, Zhejiang, PR China

ARTICLE INFO

Article history:
Received 28 September 2011
Received in revised form 23 October 2011
Accepted 25 October 2011
Available online 10 November 2011

Keywords:
Fe_3O_4
Graphene
Lithium-ion batteries
Solvothermal

ABSTRACT

A facile single step solvothermal route has been developed to prepare a composite of Fe_3O_4 nanoparticles and graphene nanosheets. The synthetic protocol takes advantage of the ethylene glycol assisted partial reduction of Fe^{3+} species to form Fe_3O_4, the reduction of graphene oxide into graphene, and the preferential attachment of fine Fe_3O_4 nanoparticles onto graphene sheets in one step. No additional reductive agent or calcination step is needed, which favors an effective, operationally simple and low-cost preparation process. The cycling properties of Fe_3O_4/graphene nanocomposite have been evaluated by galvanostatic charge–discharge measurements. The effect of graphene additive ratios on electrochemical performance has been investigated. The results show that the nanocomposite with a moderate graphene content of 18.5 wt% integrates high reversible capacity and good cyclic stability, delivering a capacity of 750 mAh/g after 40 cycles at 50 mA/g.

1. Introduction

Since the pioneering work of Tarascon et al., transition metal oxides have been particularly attractive as promising anode materials for rechargeable lithium-ion batteries (LIBs), owning to their high theoretical capacities (700–1000 mAh/g, compared with 372 mAh/g of commercial graphite anodes) [1]. Among these transition metal oxides, Fe_3O_4 has been widely investigated and considered as one of the most important candidates for next generation lithium-ion battery anode materials [2–6]. Fe_3O_4 can react with eight lithium ions per formula unit with a reversible capacity of about 926 mAh/g [2,7,8]. Compared with other transition metal oxides, Fe_3O_4 shows higher specific capacity, eco-benignity, natural abundance and higher electronic conductivity [3,8]. However, the practical application of Fe_3O_4 based electrodes has been delayed by the poor cyclic stability during the continuous charge/discharge cycling. This problem is mainly attributed to the drastic volume change in the repeated insertion/desertion of Li-ions based on the conversion mechanism. The huge volume change can cause the crushing of electrodes, leading to the electrical disconnection between anode materials and current collectors [8–10]. Another problem is the severe agglomeration of active materials, which leads to the reduction of active surface area [10]. To alleviate these problems, great efforts have been made to prepare magnetite-based nanostructures and nanocomposites [2,3,8,11–13]. Among these approaches, carbon coating has been proved to be efficient to improve the cyclic performance of magnetite [2,8]. The carbon coating serves as a buffer to relieve the volume change and preserve the electrode integrity, enhancing the electrical conductivity and electrochemical performance [9–15].

Graphene, a new allotrope of carbon, is a single atom thick two-dimensional crystal consisting of sp^2 hybridized carbon atoms, exhibiting outstanding in-plane electrical conductivity and extraordinary mechanical properties [16–18]. The unique physical and chemical properties of graphene have attracted much attention for the application in energy storage and conversion systems. Graphene hybridized nanocomposites as LIBs electrodes have been extensively studied [19–24]. The preparation of magnetite/graphene nanocomposite anode materials has also been reported, and enhanced cycle performances have been achieved [9,10,14,25]. However, these approaches are complicated, involving additional reduction agents such as N_2H_4 [10], $NaBH_4$ [25] and additional calcination steps [9,14].

Here we report a solvothermal route to prepare magnetite/graphene nanocomposite, combining nano-sized magnetite particles with graphene sheets. Ethylene glycol serves as both solvent and reduction agent in the synthetic processes. Partially reduction of Fe^{3+} species to form Fe_3O_4 nanoparticles, the reduction of graphene oxide into graphene sheets, and the attachment of fine

* Corresponding author.
** Corresponding author at: Department of Chemistry, Fudan University, Shanghai 200433, PR China.
E-mail addresses: iuzp@nimte.ac.cn (Z. Liu), c.yu@uq.edu.au (C. Yu).

0925-8388/$ – see front matter.
doi:10.1016/j.jallcom.2011.10.087

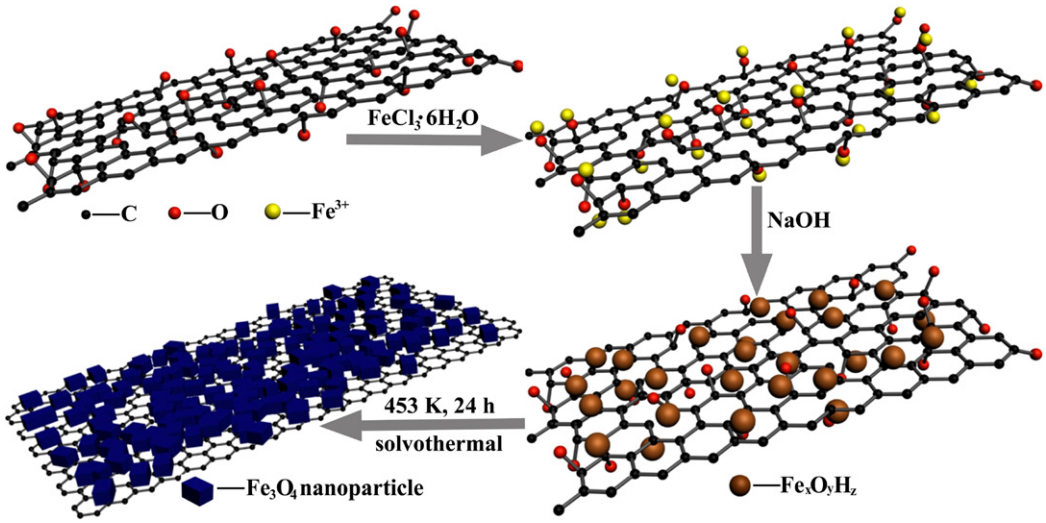

Fig. 1. A scheme for the synthesis process of Fe_3O_4/graphene nanocomposite.

Fe_3O_4 nanoparticles onto graphene sheets were achieved in one step, without additional reductive agent or further calcination step, providing an effective, simple and low-cost preparation process. By optimizing the Fe_3O_4/graphene ratios, nanocomposites with significantly enhanced cycle stability and good rate performance were obtained.

2. Experimental

2.1. Materials synthesis

Graphite oxide was prepared from graphite by the Staudenmaier method [26]. Graphite oxide (0.45 g) was dispersed into a mixed solvent (120 ml of ethylene glycol, 60 ml of H_2O and 60 ml of PEG400), then sonicated (SCIENTZ SB 3200DTN, 150 W) for 2 h to form a homogeneous graphene oxide suspension. Different amount of $FeCl_3{\cdot}6H_2O$ (0.95, 0.5 and 0.42 g) was added into the suspension at room temperature, followed by a deposition reaction with NaOH (1.76 g). After stirring for 2 h, the whole suspension was transferred into a Teflon-lined stainless steel autoclave and reacted at 180 °C for 24 h. The final product was separated by a magnet and washed extensively with water and ethanol. The samples are notated as Fe_3O_4/G-95, Fe_3O_4/G-50 and Fe_3O_4/G-42, respectively. Bare Fe_3O_4 was also synthesized by the same procedure to prepare the Fe_3O_4/graphene nanocomposite but in the absence of graphite oxide.

2.2. Characterization

Wide-angle X-ray diffraction (XRD) patterns were obtained on a Bruker D8 Advance X-ray powder Diffractometer (λ = 1.5406 Å). Raman spectrums were recorded by a Dilor LABRAM-1B Raman spectroscope, excited by 632.8 nm laser at room temperature. Transmission electron microscope (TEM) images and select area electron diffraction (SAED) pattern were obtained by a JEOL 2011 microscope operated at 200 kV. The samples for TEM measurements were suspended in ethanol and dispersed onto Cu grids with holey carbon film. Scanning electron microscopy (SEM) experiments were conducted on a Philips XL30 electron microscopy operated at 20 kV. The compositions of the Fe_3O_4/graphene nanocomposites were determined with thermal gravimetric analysis (TGA) by using a ZRY-1P thermogravimetric analyzer with a heating rate of 10 °C/min from room temperature to 750 °C under air.

The electrochemical measurements were carried out by LAND CT2001A battery testers with lithium metal as the counter electrodes at room temperature. Fe_3O_4/graphene nanocomposite was mixed with poly(vinylidene fluoride) (PVDF), at a weight ratio of 90:10 in N-methyl-2-pyrrolidone (NMP) to form a homogeneous slurry. Then, the resultant slurry was uniformly pasted on copper foil substrate with a blade. The prepared electrode sheets were placed in a vacuum oven at 80 °C to evaporate the solvent. CR2032-type coin cells were fabricated in a glove box with an argon atmosphere. The Li metal foil was used as the counter electrode. The electrolyte was 1 M $LiPF_6$ in a 50:50 w/w mixture of ethylene carbonate and diethyl carbonate. Charge–discharge cycles of the cells were measured at a constant current density of 50 mA/g in a voltage range of 0–3.0 V.

3. Results and discussion

As schematically illustrated in Fig. 1, the synthesis starts with the dispersion and exfoliation of graphite oxide in the mixed solvents to form the graphene oxide suspension. Secondly, $FeCl_3{\cdot}6H_2O$ is added as the precursor and Fe^{3+} ions are captured by oxygenous groups on the graphene oxide through coordination. After the addition of NaOH, the coordinated Fe^{3+} can be deposited by the base agent to generate $Fe_xO_yH_z$ species [27]. Finally, the Fe_3O_4/graphene nanocomposite is formed in the solvothermal treatment process by simultaneous reduction of graphene oxide to graphene and partial reduction of $Fe_xO_yH_z$ to Fe_3O_4.

The wide angle XRD patterns of graphite oxide and Fe_3O_4/graphene nanocomposite (Fe_3O_4/G-50) are shown in Fig. 2A and B, respectively. The diffraction peak centered at about 10.3° in Fig. 2A indicates a typical lamellar structure of graphite oxide with a specific interplanar distance of 0.85 nm [28]. In Fig. 2B, the absence of the peak at 10.3° suggests the complete exfoliation and reduction of graphite oxide in the ultra-sonication and solvothermal treatment [10]. Characteristic diffraction peak of graphite located at 26.4° cannot be observed neither, which indicates that no graphite-like layered structure is formed by

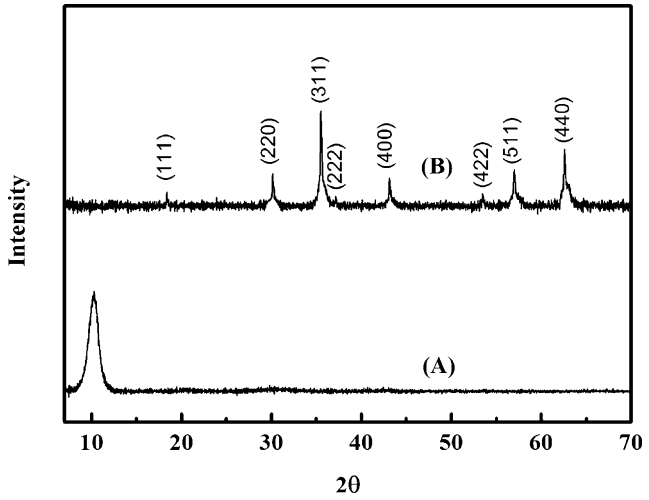

Fig. 2. Wide-angle XRD patterns of (A) graphite oxide, (B) Fe_3O_4/graphene nanocomposite (Fe_3O_4/G-50).

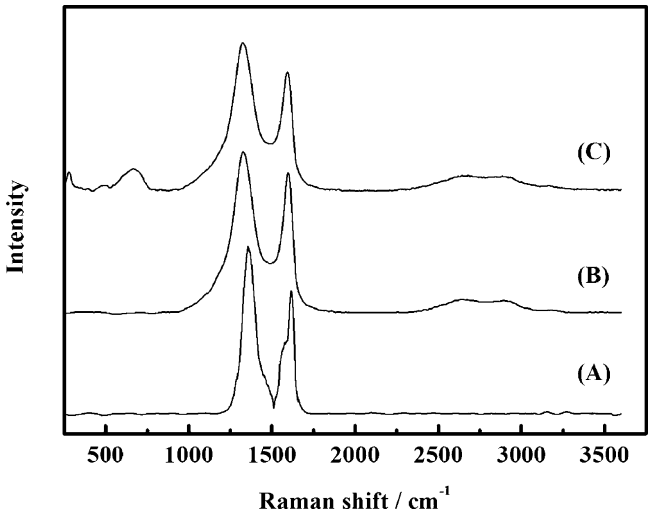

Fig. 3. Raman spectra of (A) graphite oxide, (B) graphene sheets and (C) Fe_3O_4/graphene nanocomposite (sample Fe_3O_4/G-50).

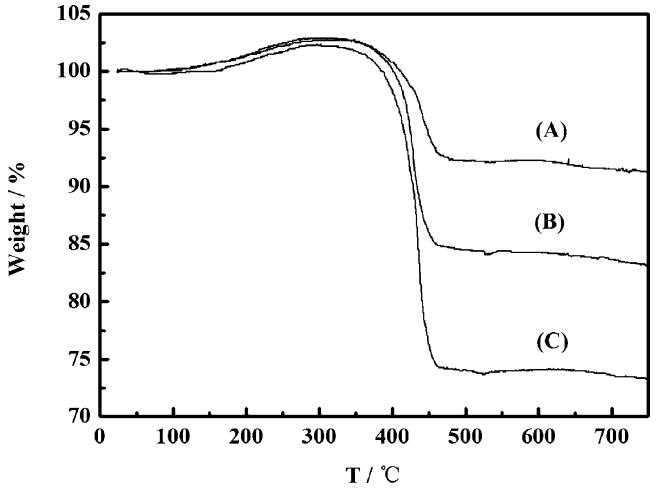

Fig. 4. TGA curves of Fe_3O_4/graphene nanocomposites, (A) Fe_3O_4/G-95, (B) Fe_3O_4/G-50, (C) Fe_3O_4/G-42.

re-stacking of chemically reduced graphene [29]. The diffraction peaks in Fig. 2B can be attributed to a face-centered cubic magnetite phase (JCPDS 75-0449). The relatively wide peak widths suggest a nanoscale size of Fe_3O_4 particles. According to the Scherrer's equation, the average particle size of Fe_3O_4 is calculated to be about 12 nm.

Fig. 3 presents the Raman spectrum of Fe_3O_4/graphene nanocomposite (Fe_3O_4/G-50), with the Raman spectra of bare graphene sheets and graphite oxide for comparison. The Raman spectrum of graphite oxide (Fig. 3A) contains only D band ($\sim$1360 cm^{-1}, for A_{1g} phonon of carbon sp^3 atoms from defects and boundaries of lattice) and G band ($\sim$1600 cm^{-1}, E_{2g} phonon of carbon sp^2 atoms) [30]. In Fig. 3B and C, new Raman scattering peaks emerged at around 2650 cm^{-1} indicate the transformation of graphite oxide to graphene nanosheets [31]. In Fig. 2C, peaks observed at about 300 cm^{-1} and 670 cm^{-1} can be attributed to the E_g and A_{1g} vibration modes of Fe_3O_4 [32,33]. The co-existence of the specific Raman peaks of both Fe_3O_4 and graphene in Fig. 2C suggests that the product is a composite of two components as designed in Fig. 1.

To quantify the amount of graphene and Fe_3O_4 components in the nanocomposites, TGA was carried out in air, with a heating rate of 10 °C/min from room temperature to 750 °C. TGA curves of three Fe_3O_4/graphene nanocomposite samples are presented in Fig. 4. As shown in the curves, the Fe_3O_4/graphene nanocomposites experienced slow mass increases between $\sim$120 °C and 350 °C, because of oxidation of Fe_3O_4 nanoparticles by gradually heating in air [34,35]. The sharp weight losses observed from 360 °C to 470 °C are mainly attributed to the decomposition of graphene nanosheets. Calculated from the weight losses of graphene and the mass gains of the oxidation of Fe_3O_4 to Fe_2O_3, the graphene contents of sample Fe_3O_4/G-95, Fe_3O_4/G-50 and Fe_3O_4/G-42 are 10.8, 18.5 and 28.3 wt%, respectively.

TEM technique was employed to study the detailed structural features of Fe_3O_4/graphene nanocomposites. TEM image at a low magnification of sample Fe_3O_4/G-50 reveals that the Fe_3O_4 nanoparticles are uniformly distributed on the basal plane of graphene nanosheets (Fig. 5a). The nanoparticles are relatively well separated and no large agglomeration can be found. The SAED image (inset of Fig. 5a) exhibits a ring-like pattern, indicating a polycrystalline nature of Fe_3O_4 nanoparticles. The diffraction rings can be indexed to (2 2 0), (3 1 1), (4 0 0) and (4 4 0) planes of a face-centered cubic magnetite phase. From the TEM image at a higher magnification (Fig. 5b), both the fringe of a graphene sheet and the morphology of Fe_3O_4 nanoparticles can be clearly observed. It also shows that Fe_3O_4 nanoparticles are anchored on graphene, which guarantees the good connection between Fe_3O_4 and graphene and ensures the effective use of conductive graphene sheets. The particle size and morphology of magnetite nanoparticles are not uniform, but most of the particles are no larger than 30 nm in size. The high resolution TEM image of a Fe_3O_4 nanoparticle is presented in the inset of Fig. 5b, in which the (111) crystal plane with a specific interplanar distance of 0.484 nm of face-centered cubic magnetite phase can be identified. SEM image of sample Fe_3O_4/G-50 also shows good hybridity of Fe_3O_4 nanoparticles and graphene sheets (Fig. S-1 in the Electronic Supplementary Material (ESM)).

Compared to TEM images of sample Fe_3O_4/G-50, sample Fe_3O_4/G-95 and sample Fe_3O_4/G-42 show different morphologies. In the TEM image of Fe_3O_4/G-95 (Fig. 5c), the surface of graphene sheets is covered by a huge amount of Fe_3O_4 nanoparticles. The superfluous Fe_3O_4 causes the overlap of nanoparticles, thus a large quantity of Fe_3O_4 nanoparticles lose direct contact with graphene. As shown in Fig. 5d, the loading amount of Fe_3O_4 on graphene is quite low in sample Fe_3O_4/G-42, in accordance with the TGA results. Fe_3O_4 nanoparticles are sparsely decorated on the graphene surface and bare graphene can be observed in many areas.

To investigate the electrochemical properties of the nanocomposites as anode materials in rechargeable LIBs, charge–discharge test was carried out using coin-type cells with a voltage cutoff of 3.0–0 V and a current density of 50 mA/g. Cyclic performance of Fe_3O_4/graphene nanocomposite samples are demonstrated in Fig. 6a, together with the result of bare Fe_3O_4 for comparison. Among three nanocomposite materials, sample Fe_3O_4/G-95 (Fig. 6a A) has the highest first discharge capacity (1470.0 mAh/g) and reversible capacity (936.0 mAh/g). However, the retention of sample Fe_3O_4/G-95 is not good enough and the capacity keeps fading to 609.4 mAh/g after 40 cycles, which can be mainly attributed to the poor connection between overloaded superfluous Fe_3O_4 nanoparticles and graphene sheets, hence the poor electric conductivity and bad volume buffering effect. Sample Fe_3O_4/G-42 exhibits relatively good stability during the continuous charge/discharge cycling (Fig. 6a C). However, the discharge capacity of the sample is kept at only 485.5 mAh/g after 40 cycling rounds, because of the low loading amount of Fe_3O_4 (10.8 wt%). Fe_3O_4/G-50 with a moderate graphene ratio (18.5 wt%) and suitable nanoparticles coverage on the graphene plane turns out to be the ideal sample which combines a high capacity (750.0 mAh/g after 40 cycles) and good

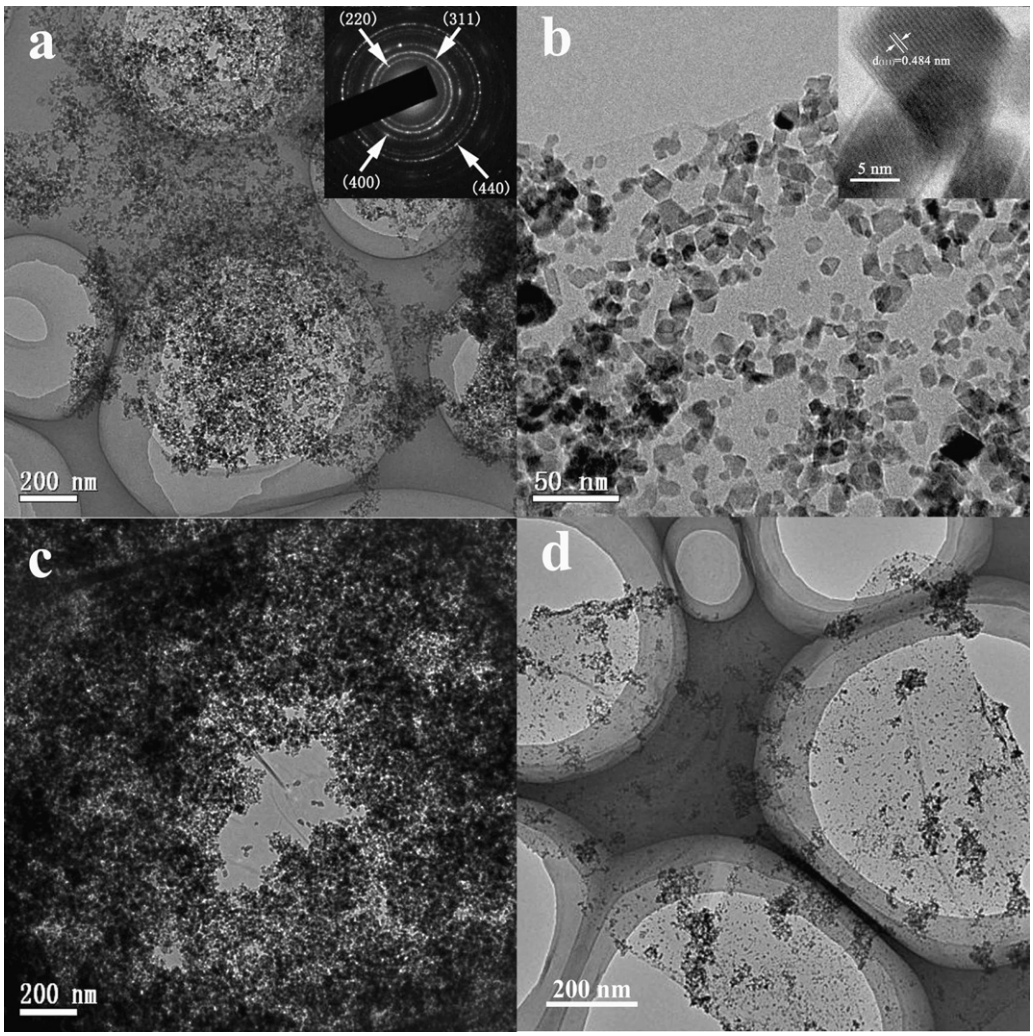

Fig. 5. TEM images of Fe_3O_4/graphene nanocomposites. (a and b) Fe_3O_4/G-50. Insert of (a) shows the selected area electron diffraction pattern. Insert of (b) shows a high-resolution TEM image of Fe_3O_4 nanoparticles, (c) Fe_3O_4/G-95. (d) Fe_3O_4/G-42.

stability (83% retention of the reversible capacity) (Fig. 6a B and Fig. S-2 in the ESM). Moreover, the coulombic efficiency of sample Fe_3O_4/G-50 keeps steady at around 99% (Fig. S-3 in the ESM). For comparison, bare Fe_3O_4 nanoparticle electrode (Fig. 6a D) exhibits very poor cycling stability, fading rapidly from 672.2 mAh/g to 65.2 mAh/g in 40 cycles.

Our results have shown that graphene modification is beneficial to the electrochemical performance of Fe_3O_4. A suitable ratio of Fe_3O_4 to graphene is also important, which gives optimized coverage of nanoparticles and ensures the integration of both the high capacity of the transition metal oxides and the excellent cycling stability improved by graphene sheets [36]. The optimum additive ratio of graphene in our work is 18.5 wt%, which is lower than that (38.0 wt%) reported by Wang et al. [10]. This discrepancy should be attributed to the differences in the synthetic methods. In Wang's case, it is assumed that graphene oxides are partially reduced by

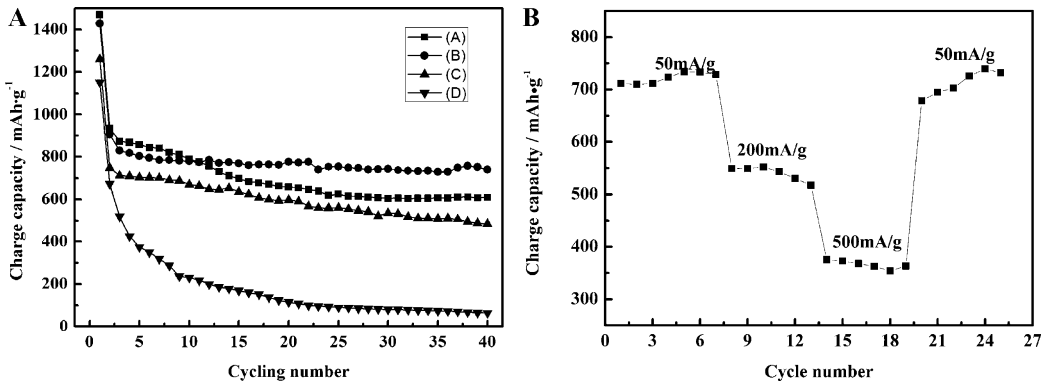

Fig. 6. (a) Cycling behavior of Fe_3O_4/graphene nanocomposites (A) Fe_3O_4/G-95, (B) Fe_3O_4/G-50, (C) Fe_3O_4/G-42 and (D) bare Fe_3O_4 nanoparticles. (b) Rate performance of Fe_3O_4/G-50.

Fe^{2+}, therefore decreasing the dispersibility of graphene oxides and leading to re-stacking. Eventually the coverage of Fe_3O_4 nanoparticles on graphene sheets is decreased and thus a higher graphene content is needed to achieve good performance (650 mAh/g after 100 cycles). However, in our method, the reduction of graphene oxide and generation of Fe_3O_4 nanoparticles happened in the same step, minimizing the re-stacking of graphene sheets, hence a lower graphene content guarantees the enhanced electrochemical properties (750.0 mAh/g after 40 cycles).

The rate performance of sample Fe_3O_4/G-50 was evaluated by carrying out charge/discharge measurements under different current densities. The discharge capacity reduces to about 550 mAh/g when the current density increases from 50 mAh/g to 200 mA/g. As the current rate reaches 500 mA/g, the discharge capacity remains stable at about 370 mAh/g, which is still comparable to commercial graphite electrodes. It is noted that a discharge capacity of ~740 mAh/g can be regained when the current density is turned back to 50 mAh/g, indicating the good stability of the nanocomposite electrode materials.

4. Conclusions

In summary, a facile single step solvothermal route to prepare Fe_3O_4/graphene nanocomposites has been developed. The synthetic strategy is mainly based on the in situ reduction of partial Fe^{3+} to form Fe_3O_4 and reduction of graphene oxide to graphene sheets in one step without additional reducing agents or calcination steps, which provides a simple, effective and low-cost method to produce Fe_3O_4/graphene nanocomposites. This one step method is also advantageous to allow for a low graphene content in the Fe_3O_4/graphene composite while the graphene sheets are homogenously coated with fine Fe_3O_4 nanoparticles, leading to a high discharge capacity of 750.0 mAh/g due to high Fe_3O_4 loading and excellent cycling stability (83% retention of the initial reversible capacity after 40 cycles) induced by volume buffering effect of graphene sheets. This optimized Fe_3O_4/graphene composite with enhanced performance may have a promising potential in the application in lithium-ion batteries.

Acknowledgements

We thank the State Key Research Program of China (2010CB226901) and the Australia Research Council for their financial supports.

Appendix A. Supplementary data

Supplementary data associated with this article can be found, in the online version, at doi:10.1016/j.jallcom.2011.10.087.

References

[1] P. Poizot, S. Laruelle, S. Grugeon, L. Dupont, J.M. Tarascon, Nature 407 (2000) 496–499.
[2] W.M. Zhang, X.L. Wu, J.S. Hu, Y.G. Guo, L.J. Wan, Adv. Funct. Mater. 18 (2008) 3941–3946.
[3] L. Taberna, S. Mitra, P. Poizot, P. Simon, J.M. Tarascon, Nat. Mater. 5 (2006) 567–573.
[4] H. Liu, G.X. Wang, J.Z. Wang, D. Wexler, Electrochem. Commun. 10 (2008) 1879–1882.
[5] J.P. Liu, Y.Y. Li, H.J. Fan, Z.H. Zhu, J. Jiang, R.M. Ding, Y.Y. Hu, X.T. Huang, Chem. Mater. 22 (2010) 212–217.
[6] F. Cheng, Z. Tao, J. Liang, J. Chen, Chem. Mater. 20 (2008) 667–681.
[7] S. Mitra, P. Poizot, A. Finke, J.M. Tarascon, Adv. Funct. Mater. 16 (2006) 2281–2287.
[8] C.M. Ban, Z.C. Wu, D.T. Gillaspie, L. Chen, Y.F. Yan, J.L. Blackburn, A.C. Dillon, Adv. Mater. 22 (2010) E145–E149.
[9] G.M. Zhou, D.W. Wang, F. Li, L.L. Zhang, N. Li, Z.S. Wu, L. Wen, G.Q. Lu, H.M. Cheng, Chem. Mater. 22 (2010) 5306–5313.
[10] J.Z. Wang, C. Zhong, D. Wexler, N.H. Idris, Z.X. Wang, L.Q. Chen, H.K. Liu, Chem. Eur. J. 17 (2011) 661–667.
[11] T. Muraliganth, A.V. Murugan, A. Manthiram, Chem. Commun. 736 (2009) 0–7362.
[12] L. Wang, Y. Yu, P.C. Chen, D.W. Zhang, C.H. Chen, J. Power Sources 183 (2008) 717–723.
[13] S.Q. Wang, J.Y. Zhang, C.H. Chen, J. Power Sources 195 (2010) 5379–5381.
[14] L.W. Ji, Z.K. Tan, T.R. Kuykendall, S. Aloni, S.D. Xun, E. Lin, V. Battaglia, Y.G. Zhang, Phys. Chem. Chem. Phys. 13 (2011) 7139–7146.
[15] J.S. Chen, Y.M. Zhang, X.W. Lou, ACS Appl. Mater. Interfaces 3 (2011) 3276–3279.
[16] M.J. Allen, V.C. Tung, R.B. Kaner, Chem. Rev. 110 (2010) 132–145.
[17] D. Chen, L.H. Tang, J.H. Li, Chem. Soc. Rev. 39 (2010) 3157–3180.
[18] M. Pumera, Chem. Soc. Rev. 39 (2010) 4146–4157.
[19] S.M. Paek, E. Yoo, I. Honma, Nano Lett. 9 (2009) 72–75.
[20] J.K. Lee, K.B. Smith, C.M. Hayner, H.H. Kung, Chem. Commun. 46 (2010) 2025–2027.
[21] S.B. Yang, X.L. Feng, L. Wang, K. Tang, J. Maier, K. Mullen, Angew. Chem. Int. Ed. 49 (2010) 4795–4799.
[22] D.H. Wang, D.W. Choi, J. Li, Z.G. Yang, Z.M. Nie, R. Kou, D.H. Hu, C.M. Wang, L.V. Saraf, J.G. Zhang, I.A. Aksay, J. Liu, Acs Nano 3 (2009) 907–914.
[23] S.J. Ding, D.Y. Luan, F.Y.C. Boey, J.S. Chen, X.W. Lou, Chem. Commun. 47 (2011) 7155–7157.
[24] S.J. Ding, J.S. Chen, D.Y. Luan, F.Y.C. Boey, S. Madhavi, X.W. Lou, Chem. Commun. 47 (2011) 5780–5782.
[25] B.J. Li, H.Q. Cao, J. Shao, M.Z. Qu, J.H. Warner, J. Mater. Chem. 21 (2011) 5069–5075.
[26] J.R. Lomeda, C.D. Doyle, D.V. Kosynkin, W.F. Hwang, J.M. Tour, J. Am. Chem. Soc. 130 (2008) 16201–16206.
[27] M. Zhang, D.N. Lei, X.M. Yin, L.B. Chen, Q.H. Li, Y.G. Wang, T.H. Wang, J. Mater. Chem. 20 (2010) 5538–5543.
[28] Y.L. Zhang, L. Guo, S. Wei, Y.Y. He, H. Xia, Q.D. Chen, H.B. Sun, F.S. Xiao, Nano Today 5 (2010) 15–20.
[29] P.C. Lian, X.F. Zhu, H.F. Xiang, Z. Li, W.S. Yang, H.H. Wang, Electrochim. Acta 56 (2010) 834–840.
[30] A.C. Ferrari, J. Robertson, Phys. Rev. B 61 (2000) 14095–14107.
[31] A.C. Ferrari, J.C. Meyer, V. Scardaci, C. Casiraghi, M. Lazzeri, F. Mauri, S. Piscanec, D. Jiang, K.S. Novoselov, S. Roth, A.K. Geim, Phys. Rev. Lett. 97 (2006), 187401(1)–187401(4).
[32] D.L.A. deFaria, S.V. Silva, M.T. deOliveira, J. Raman Spectrosc. 28 (1997) 873–878.
[33] H. Cohen, A. Gedanken, Z.Y. Zhong, J. Phys. Chem. C 112 (2008) 15429–15438.
[34] L.C.A. Oliveira, R. Rios, J.D. Fabris, V. Garg, K. Sapag, R.M. Lago, Carbon 40 (2002) 2177–2183.
[35] J.P. Sanders, P.K. Gallagher, J. Thermal Anal. Calorim. 72 (2003) 777–789.
[36] X.Y. Wang, X.F. Zhou, K. Yao, J.G. Zhang, Z.P. Liu, Carbon 49 (2011) 133–139.